Chapter 7

Potentiometric, Amperometric, and Impedimetric CMOS Biosensor Array

Kazuo Nakazato

Additional information is available at the end of the chapter

http://dx.doi.org/10.5772/53319

1. Introduction

In view of the growing concerns about such issues as food security, health care, evidence-based care, infectious disease, and tailor-made medicine, a portable gene-based point-of-care testing (POCT) system is needed. For a system that anyone can operate anywhere and obtain immediate results, a new biosensor chip must be developed. Electrical detection using complementary metal-oxide semiconductor (CMOS) integrated circuits has great potential since it eliminates the labeling process, achieves high accuracy and real-time detection, and offers the important advantages of low-cost, compact equipment.

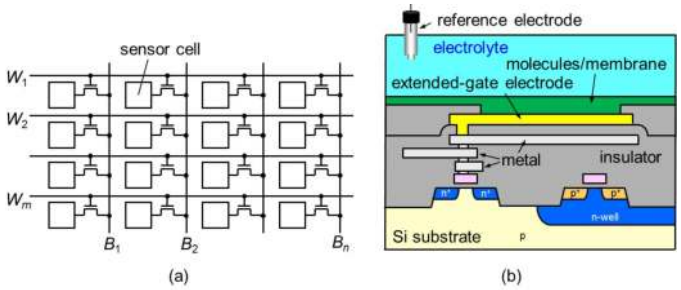

Figure 1. Integrated sensor array. (a) Matrix array arrangement where *W* and *B* are word and bit lines, respectively. (b) Schematic cross section of a sensor cell where n^+ and p^+ are heavily doped n-type and p-type semiconductors, respectively, and n-well is the n-type semiconductor region.

Our target is a monolithically integrated sensor array, as shown in Figure 1(a), which detects all possible biomolecular interactions simultaneously. In each sensor cell, different kinds of

probes can be formed for parallel detection. In addition, the same kind of probe can be used to observe the time evolution of the spatial distribution of biomolecular interactions as well as to improve the detection accuracy since biomolecular interactions are a stochastic process. In this paper, several biosensor arrays are described based on the detection of electric potential, current, capacitance, and impedance.

2. Potentiometric sensor array

The detection of electric potential change based on a field-effect transistor (FET) [1] has shown excellent sensitivity such as for ion concentration and specific DNA sequences including single-nucleotide polymorphisms (SNPs). There are two detection principles.

One principle is the detection of electronic charge around an electrode and there is no electron transfer to the electrode. The gate potential is determined by Poisson's equation. First, a probe layer is formed on an FET. Then, target molecules are supplied. Specific molecules are selectively taken into the probe layer on the FET channel, which detects the molecular charge in the probe layer. In the case of DNA detection, the probe is single-stranded (ss) DNA with a known sequence, immobilized on the substrate. When the target ssDNA is supplied, specific hybridization occurs if the target DNA is complementary to the probe DNA. Occurrence or nonoccurrence of specific hybridization can be detected by the difference in charge since a nucleotide has a negative charge on the phosphate group.

The other principle is the detection of chemical equilibrium potential, i.e., redox potential, accomplished by electron exchange between the electrolyte/molecule and the electrode. Ferrocenyl-alkanethiol immobilized gold electrode is used to detect an enzyme reaction through a redox reaction. In this case, the gate potential is determined by the Nernst equation.

2.1. CMOS Source-Drain Follower

For the integrated sensor array, the structure must be compatible with CMOS integrated circuits. Employment of extended-gate electrodes is one solution, as shown in Figure 1(b). Molecules and/or membrane are formed on the extended-gate electrodes. Our goal is the realization of a million-sensor array on a single chip. One sensor must occupy a small area, and consume low power. Since the detection signal is in the order of 1 mV, high accuracy is essential. To meet these targets, we proposed a new integrated sensor circuit, a CMOS source-drain follower, where both the gate-source and gate-drain voltages of the sensor transistor are maintained at constant values [2, 3]. The source-drain follower has the merit of not influencing the sensing system since the input impedance is infinite for both DC and AC signals.

The basic circuitry of the CMOS source-drain follower is shown in Figure 2(a). The sensor transistor N detects the extended-gate electrode voltage V_{IN}. This circuit works as a voltage follower ($V_{OUT} = V_{IN}$) with high input and low output impedances. A benefit of the voltage follower is that the output voltage is independent of device parameters such as threshold voltage and environmental conditions such as temperature. This circuit also works as a source-drain follower for sensor transistor N when current I is kept constant.

http://dx.doi.org/10.5772/53319

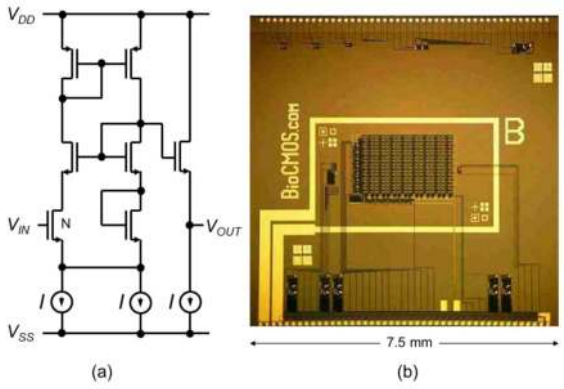

Figure 2. (a) Basic CMOS source-drain follower. V_{DD} and V_{SS} are high and low power supply voltages, respectively. (b) 16×16 integrated sensor array with CMOS source-drain followers and peripheral circuits. A heater and thermometer are also integrated on the chip.

2.2. pH Detection

Many different biosensors have been developed based on pH sensors since various biomolecular interactions produce protons. Rothberg et al. recently demonstrated a genome sequencing chip that contains 13 million pH sensors on a 17.5×17.5 mm^2 die [4].

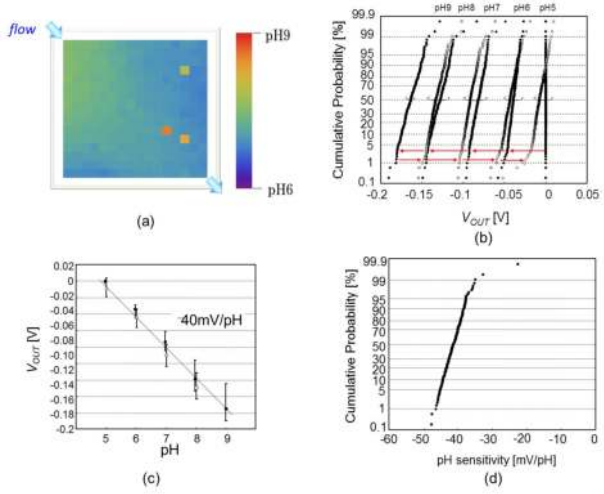

Figure 3. (a) Two-dimensional image of pH change. There are three faulty sensor units. (b) Cumulative probability of output voltage, and (c) median ±3σ plot as a function of pH from pH 5 to 9 (black) and pH 8 to 5 (white). The output voltage is the result after subtracting the initial values in order to eliminate the charge effect from the floating gate. (d) Cumulative probability of pH sensitivity of individual sensor cells.

The cumulative probability of pH sensitivity of 16×16 sensor cells with a 100-nm catalytic chemical vapor deposition (Cat-CVD) silicon nitride layer is plotted in Figure 3. Cat-CVD is a low-temperature (350°C) process and the deposited silicon nitride is of high quality, similar to that obtained by low-pressure CVD [5]. The median pH sensitivity is −41 mV/pH, which is lower than the theoretical value of −57 mV/pH. The reason for this lower value may be explained by the oxygen-rich layer on the Si_3N_4 surface [5].

2.3. DNA Detection

Using the integrated potentiometric sensor array, preliminary experiments on DNA detection were performed. Gold extended-gate electrodes were used to immobilize the probe DNA. Immobilization of a 5'-thiol-modified 20-mer oligonucleotide, and hybridization with the complementary oligonucleotide were detected in a 1 mM phosphate buffer (pH 7.0), as shown in Figure 4. Biomolecular interactions were observed as the time evolution of two-dimensional distribution. Maximum voltage change was 80 mV for immobilization and 40 mV for hybridization. In this experiment, the uniformity of biomolecular interactions was not good. Long-term drift of the sensed voltage was observed as 30 mV/h.

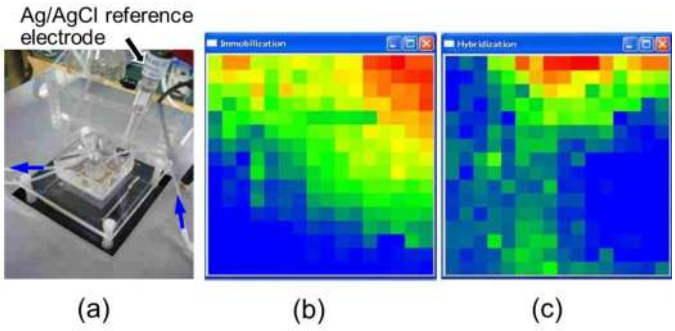

Figure 4. Preliminary experiment on DNA detection using a 16×16 potentiometric sensor array. (a) Experimental set-up. (b) Output voltage change before/after immobilization and (c) before/after hybridization.

The drift was reduced to 2 mV/h when Cat-CVD silicon nitride was deposited on the extended-gate electrode. DNA detection was also performed using the silane-coupling method for probe immobilization on Cat-CVD silicon nitride. The results show voltage changes of around 100 mV for probe immobilization, 12 mV for hybridization of complementary target DNA, and less than 1 mV for reverse-complementary target DNA.

2.4. Redox Potential Detection

The direct charge detection method using FET had a number of serious problems, as explained in Figure 5. First, the molecular charge is screened by ions in solution. Screening length is around 3 nm in the case of ion concentration of 10 mM. This can be extended if low ion

http://dx.doi.org/10.5772/53319

concentration is used; however, in this case, a very high impedance environment is produced, and the electric potential becomes unstable. Second, the charge distribution is influenced by the shape of the molecule. It is generally understood that single-stranded DNA takes a Gaussian shape, and double-stranded DNA takes a rod-like shape. It is unclear whether it is a change in charge or change in structure that is detected. Especially in a flow system, the molecular shape fluctuates, which leads to unstable electric potential. Third, the electrode enters a floating state. Embedded charge causes a large threshold voltage variation.

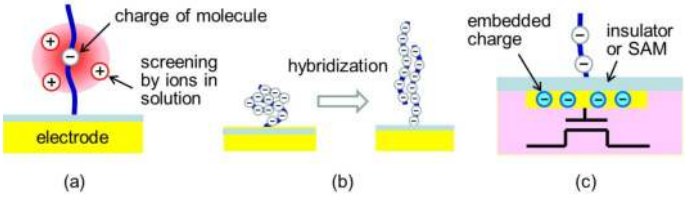

Figure 5. Problems with direct charge detection method. (a) Molecular charge is screened by ions in solution, (b) charge distribution is influenced by the shape of the molecules, and (c) electrode enters a floating state.

Instead of using the direct charge detection method, a redox potential detection method was developed using ferrocenyl-alkanethiol modified gold electrode [6, 7]. This redox potential sensor detects the ratio of oxidizer to reducer concentration, as shown in Figure 6, and is not affected by the absolute concentration and pH.

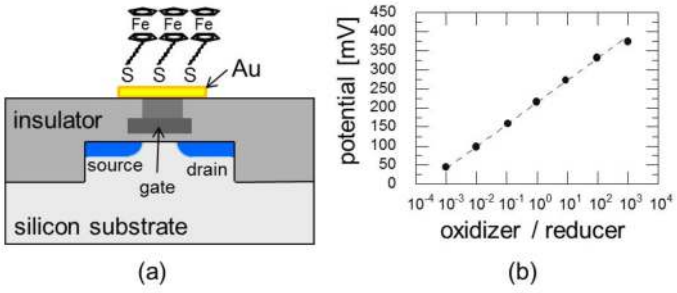

Figure 6. a) Schematic cross section of redox potential sensor. (b) Potential versus ratio of oxidizer (ferricyanide) to reducer (ferrocyanide) concentration.

We fabricated a chip that integrates 32×32 redox potential sensors, as shown in Figure 7 [8]. The sensor chip was dipped in 500 μM 11-ferrocenyl-1-undecanethiol (11-FUT) in ethanol for 24 h. Hexacyanoferrate mixture totaling 10 mM was used for the oxidizer and reducer. Six orders of concentration ratio of oxidizer and reducer were detected by this sensor array, as shown in Figure 6(b). The sensitivity was 57.9 mV/decade, which is very close to the theoretical value of 59 mV/decade at 25°C. Stability, i.e., long-term drift and fluctuation, of elec-

tric potential was examined using a bare electrode and an 11-FUT modified electrode, and 10 mM PBS solution (pH 7.4) and redox PBS solution in which the 10 mM hexacyanoferrate was additionally added to 10 mM PBS solution, as shown in Figure 7. By using redox PBS solution, the drift of electric potential was reduced by nearly one order. Furthermore, 11-FUT modification reduced the drift to nearly one fourth. This experiment showed that the drift can be drastically reduced by the redox potential detection method compared to the direct charge detection method. Of all 32×32 sensor cells, each potential of 92% was within ±1mV from the median. For the 8% abnormal output sensor cells, microscopic observation showed that an Au electrode had peeled off.

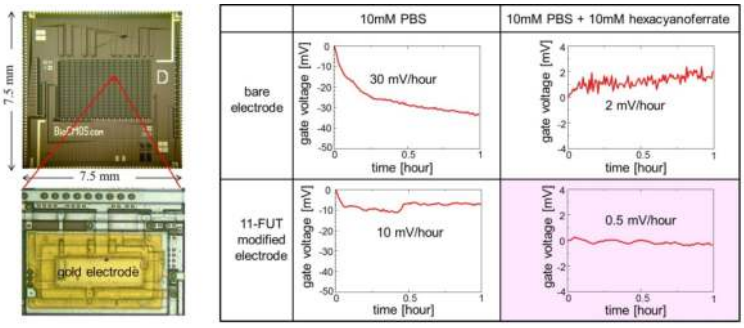

Figure 7. Redox potential sensor array (32×32) and stability of electric potential.

This redox potential sensor array successfully detected the glucose level with an accuracy of 2 mg/dL, using the following enzyme-catalyzed redox reaction:

$$\begin{aligned} &\textit{Glucose} + \textit{ATP} \xrightarrow{\text{HK}} \textit{Glucose - 6 - Phosphate} + \textit{ADP} \\ &\textit{Glucose - 6 - Phosphate} + \textit{NAD} \xrightarrow{\text{G6PDH}} \textit{Gluconolactone - 6 - phosphate} + \textit{NADH} \\ &2[\mathrm{Fe(CN)_6}]^{3-} + \textit{NADH} \xrightarrow{\text{Diaphorate}} 2[\mathrm{Fe(CN)_6}]^{4-} + \textit{NAD} \end{aligned} \tag{1}$$

where HK is hexokinase and G6PDH is glucose-6-phosphate dehydrogenase.

Continuous sample measurement was performed using a flow measurement system with a flow speed of 1 μl/s, as shown in Figure 8. We used two types of solutions: PBS solution (pH 7.4) and glucose sample solution (glucose, 9.9 mM potassium ferricyanide, 0.1 mM potassium ferrocyanide, 0.6 mM NAD, 2 mM ATP, 10 mM $MgCl_2$). PBS solution was used to wash out the glucose sample. As shown in Figure 9(a), the gate voltage settled in the glucose sample very rapidly. On the other hand, in the PBS solution, a long settling time was observed. Figure 9(b) shows the relationship between given and detected glucose concentrations, indicating fairly good linearity.

http://dx.doi.org/10.5772/53319

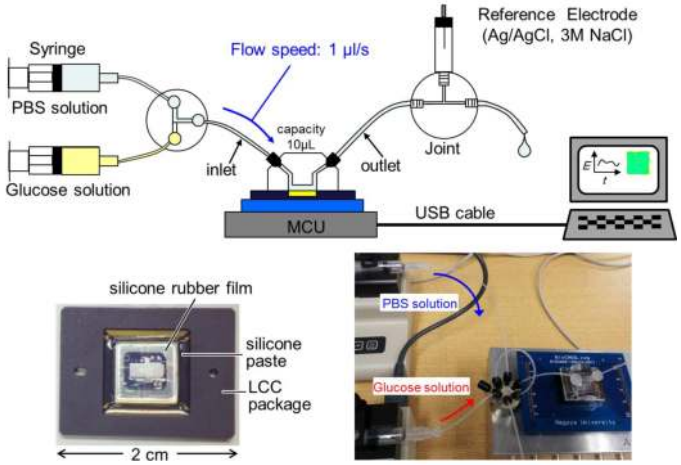

Figure 8. Setup of measurement. The chip is controlled by a microcontroller unit (MCU).

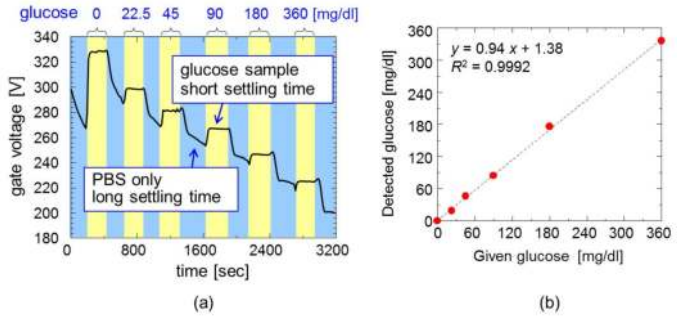

Figure 9. a) Flow measurement of glucose. Blue areas indicate the flow of PBS solution, and yellow areas indicate the flow of glucose sample solution. (b) Detected glucose vs. given glucose.

This sensor array could be applied to genome sequencing by incorporating a primer extension reaction, which produces pyrophosphate (PPi).

$$
\begin{aligned}
&PPi + H_2O \rightarrow 2Pi \\
&Pi + GAP + NAD \xrightarrow{\text{G6PDH}} 1,3BPG + NADH \\
&2[Fe(CN)_6]^{3-} + NADH \xrightarrow{\text{Diaphorate}} 2[Fe(CN)_6]^{4-} + NAD
\end{aligned}
\tag{2}
$$

where GAP is glyceraldehyde 3-phosphate and BPG is bisphosphoglycerate.

3. Amperometric sensor array

Amperometric imaging offers great potential for multipoint rapid detection and the analysis of diffusion processes of target molecules. The microelectrode is one of the most versatile and powerful tools in amperometry. Although the current passing through a microelectrode is very small, it has the advantages of high mass transport density, small double-layer capacitance, and small ohmic drop. Moreover, a microelectrode has a steady-state current response in unstirred solutions. Such steady-state currents are easy to analyze and interpret. However, as it takes a few or tens of seconds before reaching a steady state, rapid multipoint measurement cannot be achieved with a simple switching scheme. Furthermore, when the inter-electrode distance is not sufficiently large, the diffusion layers begin to overlap and eventually merge to form a single planar diffusion layer. This overlapping of diffusion layers is commonly referred to as "cross talk" or the "shielding" effect. When cross talk occurs, the microelectrode array loses its unique features and becomes similar to a large-area "macro" electrode, which makes local and quantitative analysis extremely difficult. We proposed a switching circuit that measures multiple microelectrode currents at high speed, and a microelectrode structure to suppress diffusion layer expansion over the microelectrode array [9].

3.1. Switching Circuit and Microelectrode Array Structure

Figure 10(a) shows the proposed amperometric electrochemical sensor circuit. Multiple electrodes placed in an array are connected with one amperometric sensor circuit through the switches. Each electrode is connected to two switches. The electrode being measured is connected to the readout circuit via switch SWA, and on stand-by, the potential is fixed via switch SWB to maintain the steady-state current. When the reading electrode is switched, either switch of the two is kept closed. Therefore, the switching is carried out while the steady-state current is maintained. In this way, it is not necessary to wait for a steady-state current, thus realizing ultra-fast readout from each electrode.

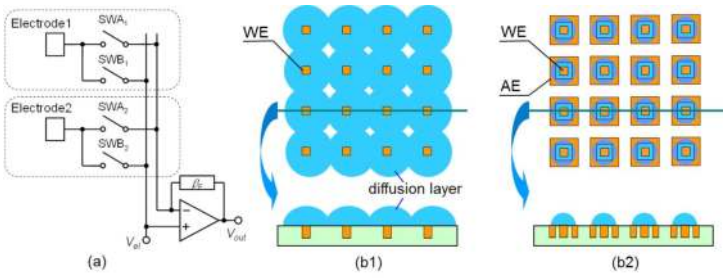

Figure 10. a) Amperometric electrochemical sensor circuit. Each electrode is connected to two switches. (b) Conventional and proposed electrode geometry.

Our working electrode (WE) structure shown in Figure 10(b2) is surrounded by a grid auxiliary electrode (AE), and the redox reaction opposite the working electrode (WE) occurs in

http://dx.doi.org/10.5772/53319

the AE. Therefore, the diffusion layer is confined around the WE, and the overlap is decreased. The steady-state current is amplified by redox cycling, and the time to reach the steady-state is reduced.

3.2. Fabricated Amperometric Sensor Array

A 16×16 amperometric sensor array was fabricated as shown in Figure 11. Ag/AgCl and Pt wire were used as reference and counter electrodes, respectively. The solution was composed of 100 mM sodium sulfate and 1 mM potassium ferrocyanide. The WE and the AE potential were fixed at 0.65 V and 0 V (vs Ag/AgCl), respectively. Figure 11 shows the current responses of 1 mM $[Fe(CN)_6]^{4-}$ observed at the single microelectrode, conventional microelectrode array, and proposed microelectrode array. This amperometric sensor array could be applied to genome sequencing by using allele-specific primers and electrochemical reaction [10].

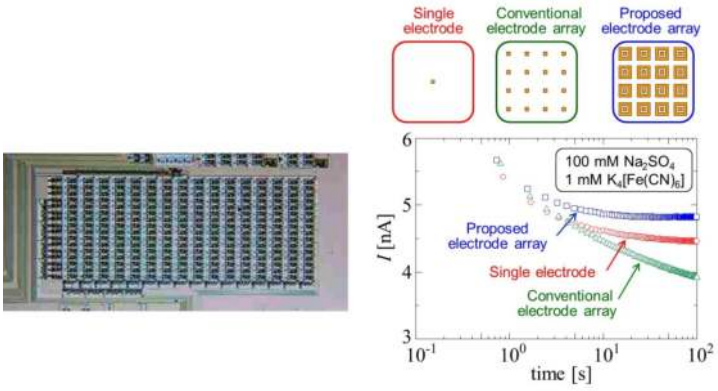

Figure 11. Amperometric sensor array (16×16) and current responses of fabricated microelectrodes. The size of the working electrode is 25×25 μm².

4. Impedimetric sensor array

4.1. Capacitance Sensor Array

We applied nonfaradaic impedimetric measurement by implementing charge-based capacitance measurement (CBCM) to realize a label-free, fully integrated capacitance biosensor. The proposed sensor exploits the capacitance changes of electrical double-layer properties as a result of biorecognition events at the sensing electrode/solution interface. Figure 12(a) shows a schematic of the proposed circuit [11]. To overcome the trade-offs between sensor area and performance, we employed a fully differential measurement circuit that would compensate for parasitic capacitances and reduce the effect of electronic noise, leading to

improvement of the detection limit. A photomicrograph of the fabricated chip is shown in Figure 12(b).

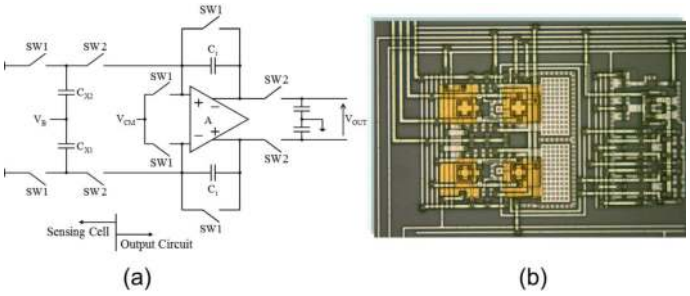

Figure 12. a) Schematic of a fully differential capacitance sensor. C_{X1} is the capacitance due to molecules to be detected. (b) Photomicrograph of a sensor chip with 4×4 μm² planar electrodes.

When probe oligonucleotides were immobilized on the electrode surface, a self-assembled monolayer serving as an insulator was formed in conjunction with the electrical double layer. The resulting interfacial capacitance is a total of these series capacitances. When complementary oligonucleotides were introduced to the probes, hybridization occurred and this interface property, i.e., double-layer thickness due to ion displacement, was altered, causing the corresponding capacitance to undergo further change. DNA detection is demonstrated by comparing the results of the capacitance measurements using bare, immobilized, and hybridized electrodes [11]. As observed in Figure 13, the immobilization gave rise to a maximum of 50% capacitance reduction when 20-mer thiolated oligonucleotides were self-assembled at the gold electrode surface. A further 20% reduction in capacitance is also observed after hybridization, implying that the double layer has changed due to the hybridization event.

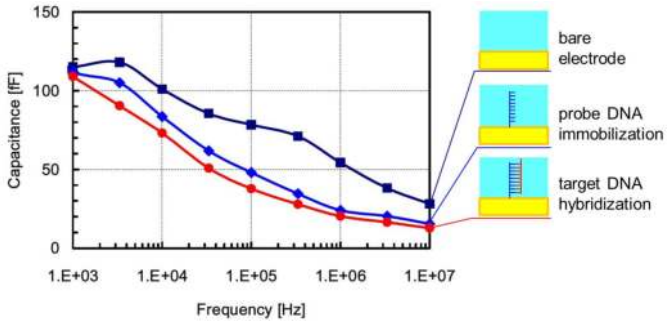

Figure 13. Measured results of capacitance against frequency for bare electrode, after DNA immobilization, and after DNA hybridization.

http://dx.doi.org/10.5772/53319

4.2. Impedance Sensor Array

Electrochemical impedance was measured between two disc electrodes of 20 mm in diameter and with 1 mm of separation, as shown in Figure 14. The specific hybridization is characterized by the change in Curie– von Schweidler exponent α of the constant phase element, which implies the structural change of molecules [12]. This shows that the overall impedance characteristic is more important than the capacitance for detecting randomly distributed molecules.

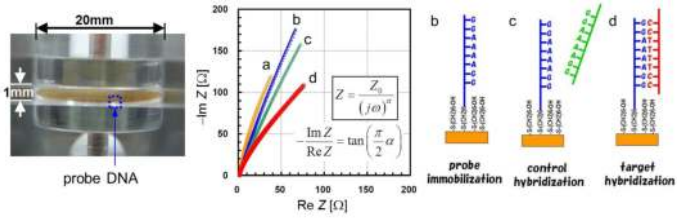

Figure 14. Electrochemical impedance spectroscopy using 20-mm-diameter Au disk electrodes, and Nyquist plot (Cole-Cole plot) of (a) bare electrode, (b) probe/mercaptohexanol immobilization, (c) electrode after noncomplementary binding, and (d) target hybridization. Impedance of constant phase element is proportional to $(j\omega)^{-\alpha}$, where j is the imaginary unit, ω is the angular frequency, and α is the Curie– von Schweidler exponent. The ratio of the imaginary part to the real part becomes a constant $-\tan(\pi\alpha/2)$.

We have designed an on-chip impedimetric sensor unit, which measures the amplitude of impedance at frequencies up to 10 MHz. The sensor unit and peripheral circuitry are shown in Figure 15. To eliminate the effect of turn-on resistance (~20 kΩ) of switch SWA and bit line capacitance (~400 fF), a current amplifier is included in each sensor unit as shown in Figure 15.

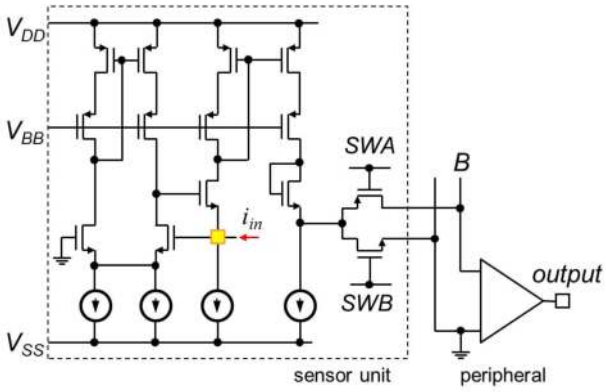

Figure 15. Circuitry of impedimetric sensor unit. AC current is amplified inside a sensor unit. V_{BB} is DC bias voltage. A similar current amplifier was used in [13].

5. Multimodal Sensor Array

In large-scale integration (LSI) circuit fabrication, the initial cost for making a set of photomasks is quite high. On the other hand, the chip cost is extremely low if a large number of chips are produced. Table 1 shows the typical cost in several technologies. From this table, more than 10,000 chips are necessary to balance the initial cost. This means that standardization and general-purpose sensor chips are important. Our strategy is to realize a multimodal sensor array for synthetic analysis and standardization. The chip consists of amperometric, potentiometric, and impedimetric smart cells containing an amplifier in the sensor cell, achieving noise reduction and not influencing the measurement system. The chip can be customized by patterning the insulator layer to cover the unused sensor cells, as shown in Figure 16.

Technology	layers	Cost of a set of photomasks	Cost of 1-cm² chip excluding photomasks
0.6 μm	2P3M	$ 30K	$ 5
0.25 μm	1P4M	$ 100K	$ 7
0.18 μm	1P6M	$ 240K	$ 9
0.13 μm	1P8M	$ 600K	$ 14

Table 1. Typical cost of LSI fabrication

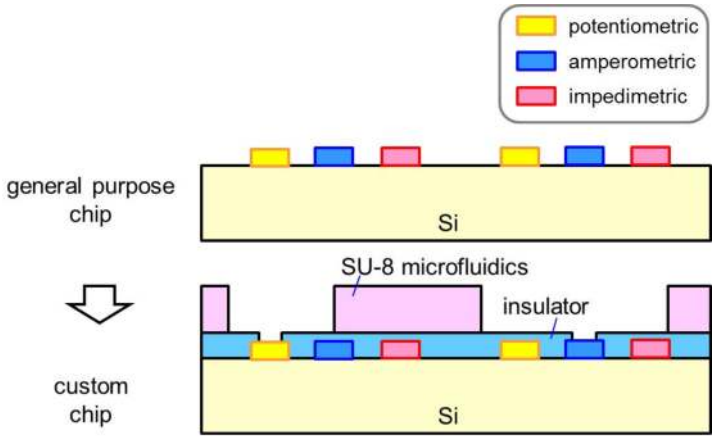

Figure 16. General-purpose sensor chip integrated with potentiometric, amperometric, and impedimetric sensor units. The chip can be customized by the post-CMOS process.

A multimodal sensor unit with potentiometric, amperometric, and impedimetric sensors is shown in Figure 17. The chip was fabricated by using a 1.2-μm 2P2M (2-polysilicon and 2

http://dx.doi.org/10.5772/53319

metal layers) CMOS process. Furthermore, a 16×16 multimodal sensor array with 0.24 mm pitch was designed using a 0.6-μm 2P3M mixed-signal general CMOS process.

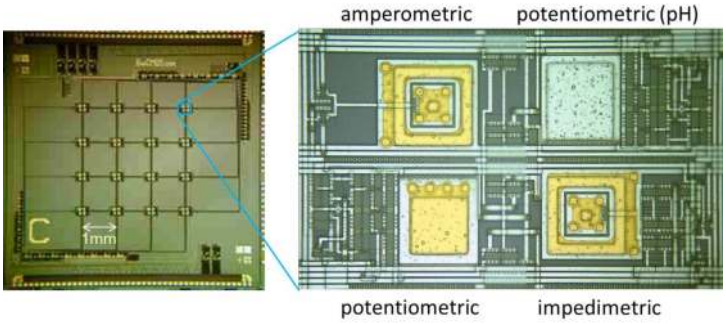

Figure 17. A 4×4 1-mm-pitch multimodal sensor array integrated with potentiometric, amperometric, and impedimetric sensor units.

6. Conclusion

Potentiometric, amperometric, and impedimetric sensor arrays using standard CMOS technology are described. Biomolecular interactions were observed as the time evolution of two-dimensional distribution. The multimodal sensor array with potentiometric, amperometric, and impedimetric sensor units will enable synthetic sensing and standardization of Bio-CMOS LSIs.

Acknowledgements

This study is based on work conducted with Mr. Hiroo Anan, Dr. Yusmeeraz Binti Yusof, and Dr. Shigeyasu Uno of Nagoya in collaboration with Dr. Masao Kamahori and Mr. Yu Ishige at the Central Research Laboratory, Hitachi, Japan. This research was financially supported by a Grant-in-Aid for Scientific Research (No. 20226009) from the Ministry of Education, Culture, Sports, Science and Technology of Japan. The fabrication of CMOS chips is supported by ON Semiconductor Technology Japan Ltd. (1.2 μm process) and TSMC (0.6 μm process), and the VLSI Design and Education Center (VDEC), University of Tokyo in collaboration with Synopsys, Inc. and Cadence Design Systems, Inc.

Author details

Kazuo Nakazato*

Address all correspondence to: nakazato@nuee.nagoya-u.ac.jp

Department of Electrical Engineering and Computer Science, Graduate of Engineering, Nagoya University, Nagoya, Japan

References

[1] Bergveld, P. (1970). Development of an ion-sensitive solid-state device for neurophysical measurements. *IEEE Trans. Biomed. Eng.;BME*, 17-70.

[2] Nakazato, K., Ohura, M., & Uno, S. (2008). CMOS cascode source-drain follower for monolithically integrated biosensor array. *IEICE Trans. Electron*, E91C-1505.

[3] Nakazato, K. (2009). Integrated ISFET Sensor Array. *Sensors*, 9-8831.

[4] Rothberg, J. M., et al. (2011). An integrated semiconductor device enabling non-optical genome sequencing. *Nature*, 475-348.

[5] Kagohashi, Y., Ozawa, H., Uno, S., & Nakazato, K. (2010). Complementary Metal-Oxide-Semiconductor Ion-Sensitive Field-Effect Transistor Sensor Array with Silicon Nitride Film Formed by Catalytic Chemical Vapor Deposition as an Ion-Sensitive Membrane. *Jpn. J. Appl. Phys*, 49-01AG06.

[6] Ishige, Y., Shimoda, M., & Kamahori, M. (2009). Extended-gate FET-based enzyme sensor with ferrocenyl-alkanethiol modified gold sensing electrode. *Biosens Bioelectron*, 24-1096.

[7] Kamahori, M., Ishige, Y., & Shimoda, M. (2008). Enzyme Immunoassay Using a Reusable Extended-gate Field-Effect-Transistor Sensor with a Ferrocenialkanethiol-modified Gold Electrode. *Anal. Sci*, 24-1073.

[8] Anan, H., Kamahori, M., Ishige, Y., & Nakazato, K. (2012). Redox-Potential Sensor Array based on Extended-Gate Field-Effect Transistors with ω-ferrocenylalkanethiol-modified Gold Electrodes. *Sens. Actuators: B. Chem.*, in press.

[9] Hasegawa, J., Uno, S., & Nakazato, K. (2011). Amperometric Electrochemical Sensor Array for On-Chip Simultaneous Imaging: Circuit and Microelectrode Design Considerations. *Jpn. J. Appl. Phys*, 50-04DL03.

[10] Tanaka, H., Fiorini, P., Peeters, S., Majeed, B., Sterken, T., de Beeck, M. O., & Yamashita, I. (2011). Sub-micro-liter Electrochemical Single-Nucleotide-Polymorphism Detector for Lab-On-a-Chip System. *Extended Abstract of 2011 ISSDM*, 1109-1110.

[11] Yusof, Y. B., Sugimoto, K., Ozawa, H., Uno, S., & Nakazato, K. (2010). On-chip Microelectrode Capacitance Measurement for Biosensing Applications. *Jpn. J. Appl. Phys*, 49-01AG05.

[12] Yusof, Y. B., Yanagimoto, Y., Uno, S., & Nakazato, K. (2011). Electrical characteristics of biomodified electrodes using nonfaradaic electrochemical impedance spectroscopy. *World Academy of Science, Engineering and Technology*, 73-295.

[13] Manickam, A., Chevalier, A., Mc Dermott, M., Ellington, A. D., & Hassibi, A. (2010). A CMOS Electrochemical Impedance Spectroscopy (EIS) Biosensor Array. *IEEE Tran. Biomed. Eng*, 4-376.